Inorganic Chemistry

Article

pubs.acs.org/IC

Hexagonal Crown-Capped Zinc Oxide Micro Rods: Hydrothermal Growth and Formation Mechanism

Lijing Zhang,[†] Xiaomiao Liu,[†,‡] Chong Geng,[†] Huajing Fang,[†] Zhipeng Lian,[†] Xiaoqing Wang,[†] Dezhong Shen,[†] and Qingfeng Yan*[,†]

[†]Department of Chemistry, State Key Laboratory of New Ceramics and Fine Processing, Tsinghua University, Beijing 100084, China

[‡]Faculty of Electronic Science and Technology, Hubei University, Wuhan 430062, China

Supporting Information

ABSTRACT: Hexagonal crown-capped ZnO micro rods were successfully prepared by a facile low-temperature hydrothermal method. The as-prepared ZnO micro rods are 4.4−5.2 μm in length and 2.4−3.6 μm in diameter, possessing a single-crystal hexagonal structure. The morphology evolution and structure changes were tracked during hydrothermal growth by field-emission scanning electron microscopy and X-ray diffraction, respectively. A three-stage growth mechanism of the hexagonal crown-capped ZnO micro rods was proposed and further verified by a growth solution renewal experiment. The room-temperature photoluminescence (PL) spectrum of the hexagonal crowns exhibits a strong UV emission at about 382 nm. The temperature dependent PL results indicate that the UV emission originates from the radiative free-exciton recombination.

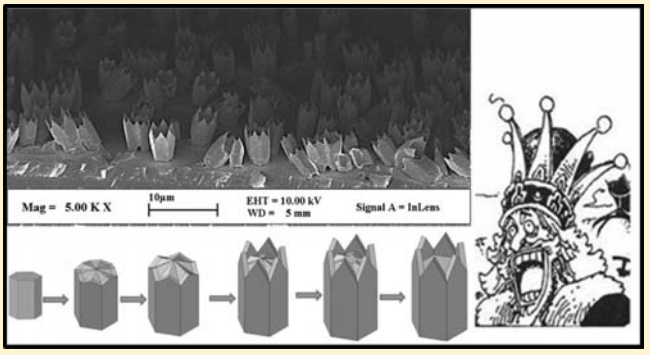

1. INTRODUCTION

Semiconductor micro/nano materials play a significant role in manufacturing electronic and optoelectric devices.[1] With the development of modern materials science and technology, much effort has been devoted to preparing one-dimensional (1D) micro/nano materials because of their unique properties and potential applications.[2] Zinc oxide (ZnO), as the II−VI semiconductor with a wide band gap (3.37 eV), high exciton binding energy (60 meV) and high efficiency of exciton recombination, has attracted much attention over the past decades. ZnO has been demonstrated to have broad applications in light emitting diodes (LEDs),[3] laser diodes, solar cells, photodetectors,[4] field-effect transistors,[5] sensors,[6] photovoltaic devices,[7] and piezoelectric devices.[8] Control over the size, shape, surface roughness, and crystallization is of great significance for the fabrication of ZnO materials since they affect their performance in practical applications. For example, ZnO has been introduced into conventional ITO-based LEDs to enhance the light extraction efficiency (LEE).[9] It was found that ZnO submicrorods with needle-like or flat end modified LEDs possess much higher LEE.[9a] Up to now, a variety of methods such as chemical vapor deposition, thermal evaporation, electrochemical deposition, and the solution-phase process have been developed to prepare the ZnO micro/nano structures.[10] Among these methods, the solution-phase process may be the simplest and effective method to prepare well-crystallized ZnO materials in facile and mild conditions.[11] A wide variety of morphologies of ZnO micro/nanostructures have been reported, including wires, belts, rods, tubes, needles, combs, forests, tetra-pods, hexagonal microboxes, dumbbells, nanobridges, nanonails, and crown-like ZnO microcrystals.[12] However, most ZnO micro/nano structures reported so far possess a needle-like or flat top morphology. Fabrication of ZnO 1D micro/nano structures with other top morphology may lead to new applications in functional devices such as LEDs and field-emission devices.

In this work, ZnO micro rods with a new top morphology, that is, a hexagonal crown-capped shape, were fabricated via a simple low-temperature hydrothermal method. We described the basic growth process and tracked the morphology evolution of the ZnO micro rods during hydrothermal growth. The morphology, crystallinity, structure, and defects of the hexagonal crown-capped ZnO micro rods were examined in detail. The formation mechanism of the hexagonal crown-capped ZnO micro rods was discussed from the viewpoint of anisotropic growth and solute transportation. A three-stage growth mechanism was proposed through observation of some intermediates at different growth stages. Furthermore, the room-temperature photoluminescence (PL) of the hexagonal crown-capped ZnO micro rods was investigated, which revealed that these ZnO micro rods showed excellent UV emission performance. The hexagonal crown-capped ZnO micro rods enrich the family of the ZnO micro/nano structures and may find potential applications in field emission devices and enhancing LEE of light emitting diodes.

Received: June 28, 2013
Published: August 20, 2013

2. EXPERIMENTAL SECTION

Materials. All chemicals, including acetone (≥99.5%), ethanol (≥99.7%), zinc nitrate hexahydate ($Zn(NO_3)_2·6H_2O$, ≥ 99.0%), and hexamethylenetetramine (HMT, ≥ 99.0%), were of analytical grade and used as received without further purification from Sinopharm Chemical Reagent Co., Ltd. Deionized (DI) water (resistivity greater than 18.2 MΩ·cm, Ultra Pure UV, China) was used in all experiments. The p-type 4-in. (100) silicon wafer (KYKY Technology Co., Ltd) used in this work was single side polished and its resistivity was 1−10 Ω·cm.

Hydrothermal Growth. The solid reactants $Zn(NO_3)_2·6H_2O$ and HMT were dissolved in DI water to prepare the growth solutions with equal concentration (0.1 M) and kept under mild magnetic stirring for 10 min. Then 80 mL of the solution was transferred into a 100 mL sealed Teflon-lined stainless-steel autoclave (dimensions: 4 × 4.4 × 9 cm^3 in inner diameter/external diameter/height). The silicon substrate (2 cm × 2 cm) was cleaned previously by a typical procedure (sonicated in acetone, ethanol, and DI water each for 10 min, then blown dry by nitrogen gas) was immersed into the growth solution with polished side down to keep any precipitates suspended in the solution body from falling down onto the substrate. The hydrothermal growth was carried out at 90 °C for 10 h. After growth, the silicon substrate was taken out and washed with DI water, and dried at 35 °C in atmosphere for further characterization.

Characterization. The morphology and microstructure of the products were observed in a field-emission scanning electron microscope (FESEM, Gemini LEO 1530). X-ray diffraction (XRD, Bruker D8-advance) was used to identify the crystalline structure. The detailed microstructure analysis was performed by the high resolution transmission electron microscopy (HRTEM, Sirion200), and the selected area electron diffraction (SAED) patterns were obtained on a FEI Tecnai G2 F20 S-Twin transmission electron microscope (TEM) with an accelerating voltage of 200 kV. Raman-scattering spectra were collected using an HR-800 (HORIBA, JY) Lab Ram confocal Raman microscope with a backscattering configuration mode. Room-temperature PL spectra were recorded on a fluorescence spectrophotometer (Hitachi, F-7000) using a Xe lamp with an excitation wavelength of 325 nm.

3. RESULT AND DISCUSSION

Morphology of the Hexagonal Crown-Capped ZnO Micro Rods. The morphology of the obtained ZnO micro rods was characterized by FE-SEM, and typical images are shown in Figure 1. Figure 1a shows the top view of the ZnO microstructure under a low resolution. It is clear that such hexagonal crown-capped ZnO micro rods can be fabricated in a large area and with a uniform size. Magnified images of the top view and side view are shown in Figures 1b and 1c, respectively. The high-resolution images show that the micro rod is a symmetrical hexagonal crown-capped structure. And the as-prepared ZnO micro rods are 4.4−5.2 μm in length and 2.4−3.6 μm in diameter, indicating an average aspect ratio of about 2 for each rod. The well-faceted hexagonal crown-capped morphology indicates that each rod is a single crystal of wurtzite ZnO with the elongation axis along the [0001] direction, which is further confirmed by XRD and TEM characterization in the following section. It is interesting that the 6 triangle nanowalls incline outward a bit on the edges of each face of the hexagonal column. The triangle nanowalls are 1.0−1.8 μm in length with a wall thickness of 100−200 nm. Six edges construct a short prismatic cup erecting on the top, leading to the hexagonal crown-capped zinc oxide micro rods. Remarkably, the inner faces of the ends look flat, while there are also some indentations highlighted by white arrows in Figure 1b which have not been completely overlapped by (0001) planes. From the side view image in Figure 1c, it can be seen that these hexagonal crown-capped micro rods are vertically oriented and well arranged on the silicon substrate.

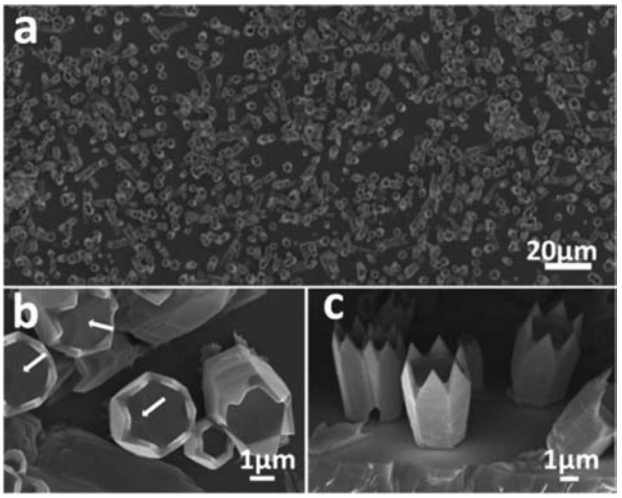

Figure 1. FE-SEM images of the hexagonal crown-capped ZnO sample. (a) Low-resolution image, (b) top view high-resolution image with the white arrows indicating indentations unlapped by (0001), and (c) side view high-resolution image.

Effect of the Reactant Concentration. When synthesizing the inorganic materials by the solution method, the concentration of reactants generally plays a significant role in controlling the morphology of the products.[12a,d,e] To figure out the effect of the reactant concentration on the formation of hexagonal crown-capped ZnO micro rods, a series of $Zn(NO_3)_2·6H_2O$ and HMT concentrations were investigated while maintaining their ratio to 1:1. The morphologies of the prepared ZnO samples under different reactant concentrations were illustrated in Figure 2. When the concentration was 0.01 M, the asymmetrical ZnO micro rods with a coarse end and a fine end were obtained (Figure 2a). As seen from the inset high-resolution image in Figure 2a, the whole ZnO micro rod is about 20 μm in length and the coarse end is about 3 μm while the fine end is 1.5 μm in diameter. When the concentration was increased to 0.05 M, symmetrical hexagonal prisms were obtained with 1.5 μm in diameter, and the end of the prisms was almost flat without any sign of crown cap. Once the concentration was increased to 0.1 M, the hexagonal crown-capped ZnO micro rods were successfully prepared, as illustrated in Figure 2c. As the concentration was further increased to 0.2 M, ZnO nanodisks with uniform size and smooth surface were obtained and interleaved with each other. It is obvious that the morphology of the obtained ZnO products was determined in large part by the reactant concentration. This is because that the higher the reactant concentration, the more ZnO nuclei appear simultaneously at the beginning of the reaction. These nuclei congregate easily and form bigger nuclei under the hydrothermal conditions, leading to the formation of bigger ZnO crystals. What is more, it was also found that with an increase in the reactant concentration the aspect ratio of the obtained ZnO samples decreased dramatically. Namely, the ZnO preferential growth direction [0001] would diminish with an increase in the reactant concentration.

Morphology Evolution. To explore the growth process of the crown-capped ZnO micro rods, the ZnO samples were collected every hour from the hydrothermal bath for FE-SEM and XRD characterization. Figure 3 shows the morphology

dx.doi.org/10.1021/ic401646t | Inorg. Chem. 2013, 52, 10167−10175

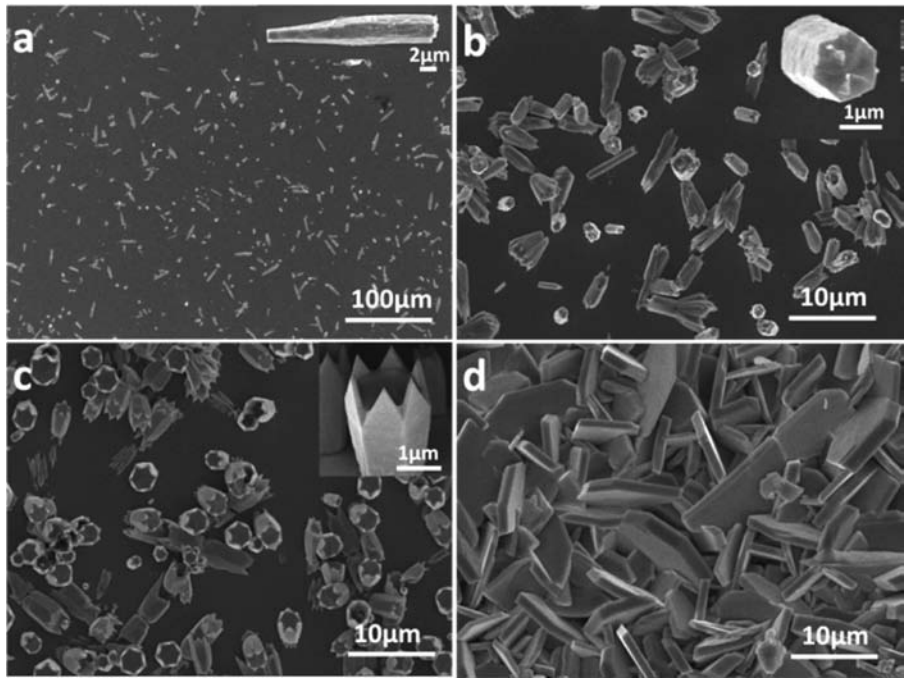

Figure 2. FE-SEM images of the ZnO samples prepared with different reactant concentrations: (a) 0.01 M, (b) 0.05 M, (c) 0.1 M, and (d) 0.2 M. The reaction time is 10 h.

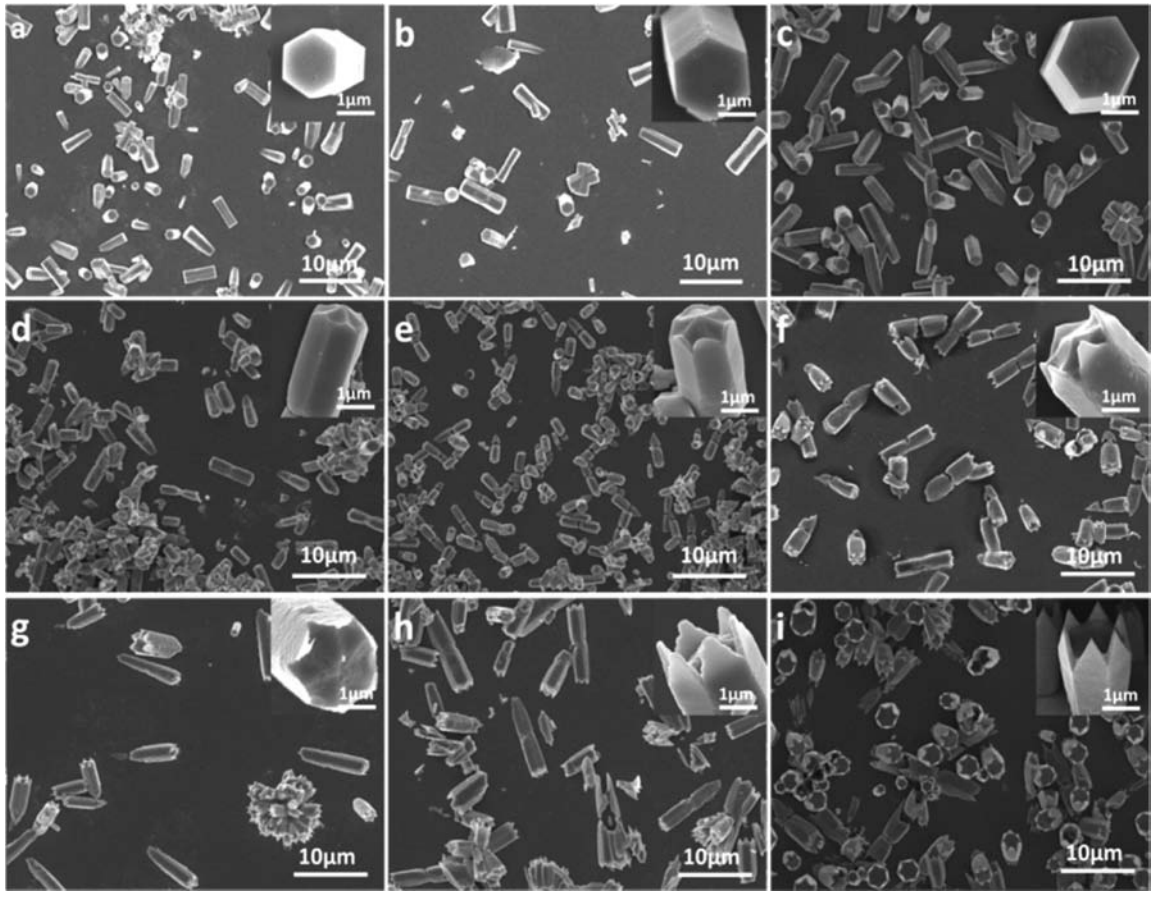

Figure 3. FE-SEM images of the ZnO samples produced at different reaction time: (a) 1 h, (b) 2 h, (c) 3 h, (d) 4 h, (e) 5 h, (f) 6 h, (g) 7 h, (h) 8 h, and (i) 10 h. The insets are the corresponding magnified images.

evolution of the ZnO micro rods aging from 1 to 10 h, and the corresponding XRD patterns are shown in Figure 5. As shown in Figure 3a, a few hexagonal prisms were obtained after incubation at 90 °C for only 1 h. They were about 1.5 μm in

dx.doi.org/10.1021/ic401646t | *Inorg. Chem.* 2013, 52, 10167−10175

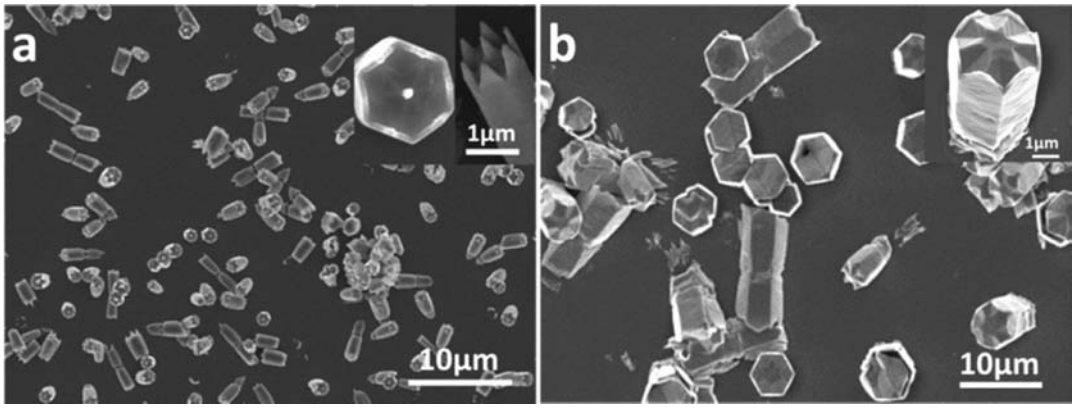

Figure 4. FE-SEM images of two ZnO intermediates prepared during the hydrothermal growth at 90 °C for about 9 h. (a) ZnO rods with a nanotip at the center of the inner fine structure. (b) ZnO rods with hexagonal star pattern covering on the inner fine structure.

diameter and 4−5 μm in length and randomly positioned on the silicon substrate. It can be observed clearly that the first 3 h of growth led to almost the same morphology (Figures 3a, 3b, and 3c). The top face of the hexagonal prisms was extremely flat without any other trace. The inset images illustrated that the ZnO micro rods grew bigger and longer with prolonged growth time. The diameter of the ZnO micro rods became 2.36 μm when the reaction proceeded to 3 h, as shown in Figure 3c. This is similar to the growth process of ZnO nanorods.[13] A morphology change occurred when the incubation time extended to 4 h. As shown in Figure 3d, the flat face of the ZnO micro rods disappeared and was replaced by a group of 12 symmetric convex and concave surfaces. The central part along [0001] direction is higher than the edges. As the reaction time was extended to 5 h, 6 convex triangle nanowalls on the edges of each plane of the hexagonal column emerged, and grew higher than the central part. Furthermore, the symmetry of the inner surfaces became increasingly evident, as illustrated in Figure 3e. When the reaction time changed from 6 to 8 h, the inner fine structure disappeared gradually and the outer triangle nanowalls became increasingly sharp (Figure 3f to 3h). Further extending the reaction time to10 h resulted in the final hexagonal crown-capped zinc oxide rods (Figure 3i), with the inner fine structure disappearing completely and a flat plane appearing in the end. The morphology evolution suggests that the ZnO micro rods with inner fine structure (Figure 3d) are only intermediates. As the reaction went on, they show up and disappear gradually and finally form the hexagonal crown-capped ZnO microstructure. The morphology evolution provides some clues for understanding the formation mechanism of the hexagonal crown-capped ZnO micro rods. It was also found that further increasing the incubation time led to the disappearance of the hexagonal crown-capped structure. For example, a porous ZnO film formed when the reaction time extended to 20 h (see Supporting Information, Figure S1). Hence, an appropriate reaction time is necessary to achieve the hexagonal crown-capped ZnO micro rods.

To track the morphology change from the original hexagonal prisms to the hexagonal crown-capped ZnO rods in more detail, a series of repetitive experiments were conducted. During the growth process of the hexagonal crown-capped ZnO micro rods, we observed two kinds of important morphologies at about 9 h, as shown in Figure 4. The ZnO rods shown in Figure 4a have a nanotip at the center of the inner fine structure. It seems that the top of the fine structure provided an active site for the second growth in the [0001] direction.[14] Figure 4b shows the ZnO rods with a hexagonal star pattern covering on the fine structure. We speculated that they may be two transition states from Figure 3h to Figure 3i. Laudise et al. reported that the (0001) plane is the most likely remaining facet regarding the growth of ZnO crystals.[15] The (0001) plane would expand gradually and overlap the fine convex and concave surfaces, finally form the hexagonal crown-capped ZnO micro rods, as shown in Figure 3i. These two structures are useful for us to understand the entire morphology evolution.

The crystallinity and crystal phase of the ZnO samples obtained at different reaction time corresponding to that shown in Figure 3 were analyzed by XRD (Figure 5). The peaks noted

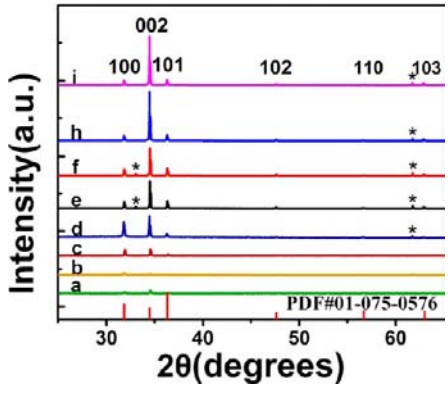

Figure 5. XRD patterns of the ZnO samples produced at different reaction times: (a) 1 h, (b) 2 h, (c) 3 h, (d) 4 h, (e) 5 h, (f) 6 h, (h) 8 h, and (i) 10 h.

by an asterisk originated from the p-type (100) silicon substrate. All the diffraction peaks of each sample can be indexed to a wurtzite structured ZnO (hexagonal phase, space group $P6_3mc$) and are in good agreement with the XRD pattern of wurtzite ZnO (PDF #01-075-0576) with lattice constants of a = 3.242 Å and c = 5.194 Å. No other phases were observed in these patterns. It is obvious that the (002) peak is the strongest one, and the intensities of the diffraction peaks increased with the reaction time. This means that a longer reaction time leads to a higher crystal quality. Combined with the geometrical shapes, we can confirm that the micro rods are single crystals with [0001] preferential growth direction, and the top and side surfaces are formed by {0001} and {10$\bar{1}$0} planes, respectively.

dx.doi.org/10.1021/ic401646t | Inorg. Chem. 2013, 52, 10167−10175

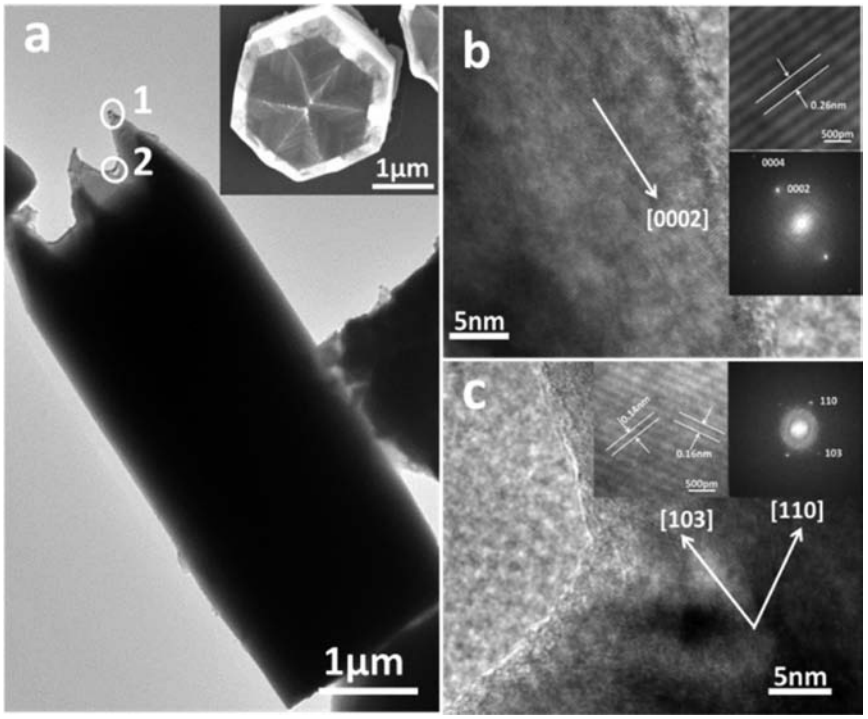

Figure 6. (a) Low magnification TEM image of the hexagonal crown-capped ZnO micro rods; the inset is a SEM image from top view. (b) HRTEM image of the circled region **1** in (a), showing the single crystallinity and the triangle nanowalls grown along [0002] (inset FFT pattern). (c) HRTEM image of the circled region **2** in (a), showing the bump planes grown along $[2\bar{1}\bar{1}3]$ and $[11\bar{2}0]$ (inset FFT pattern).

When the reaction time changed from 1 to 10 h, the intensity of peak (100) first increased and then decreased, which indicates that the growth velocity of $[10\bar{1}0]$ also underwent a corresponding change. After growth for 3 h, the (101) (102) (103) planes emerged gradually, indicating that a group of new crystal faces $\{11\bar{2}k\}$ turn up (this Miller index will be depicted in much more detail in the following section). The evolution of the XRD patterns is in agreement with the morphology changes observed from the FE-SEM images shown in Figure 3.

Structure Characterization. The detailed microstructures of the hexagonal crown-capped ZnO micro rods were further examined by the high-resolution TEM and Raman spectroscopy.

Figure 6a illustrates the low magnification TEM image of the hexagonal crown-capped ZnO micro rods. The inset in Figure 6a is a top view SEM image of the hexagonal crown-capped ZnO micro rods. The HRTEM images taken from the circled regions in Figure 6 a are shown in Figure 6b and Figure 6c, respectively. Figure 6b from region 1 focus on the outer triangle tip. The distance between the lattice fringes is 0.26 nm which corresponds to the distance of the (0002) planes, indicating that the nanowall parts grow along the [0001] crystallographic direction. The distance between the diffraction spots on the corresponding fast Fourier transform (FFT) pattern is consistent with the HRTEM results shown in the inset of Figure 6 b. The image in Figure 6c concentrates on the corner of two triangle nanowalls. The magnified images shown in the inset of Figure 6c indicate that the lattice fringes have two distances of 0.14 and 0.16 nm, corresponding to the interplanar distance of (103) and (110), respectively. Converted into four-axis coordinate, they are $[2\bar{1}\bar{1}3]$ and $[11\bar{2}0]$. The inner bump planes may grow along $[2\bar{1}\bar{1}k]$ and $[10\bar{1}0]$ directions.[16] Owing to the combined effect of these two directions, the ZnO crystal grows along 13 directions, which leads to the formation of these bump surfaces. The FFT pattern shown in the inset of Figure 6c displays two sets of diffraction spots. According to the calculation formula of the spacing, for Hexagonal:

$$d_{hkl} = \frac{a}{\sqrt{\frac{4}{3}(h^2 + k^2 + hk) + l^2\frac{a^2}{c^2}}}$$

When d_{002} = 2.6 Å, d_{110} = 0.16 Å, we can approximately calculate the lattice constants of a = 3.2 Å and c = 5.2 Å, which are consistent with the earlier XRD results.

Raman spectroscopy was also conducted to study the vibrational properties of the ZnO samples prepared at different reaction times. Here we selected ZnO samples with three typical morphologies to analyze. Figure 7 presents their Raman

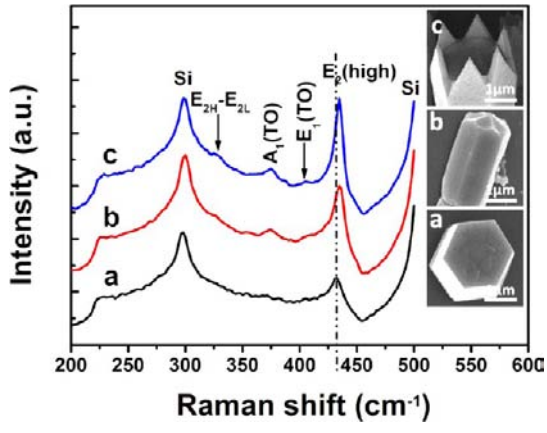

Figure 7. Raman spectra of the ZnO samples prepared at different reaction times: (a) 3 h, (b) 4 h, (c) 10 h. The excitation wavelength is 514 nm.

dx.doi.org/10.1021/ic401646t | Inorg. Chem. 2013, 52, 10167−10175

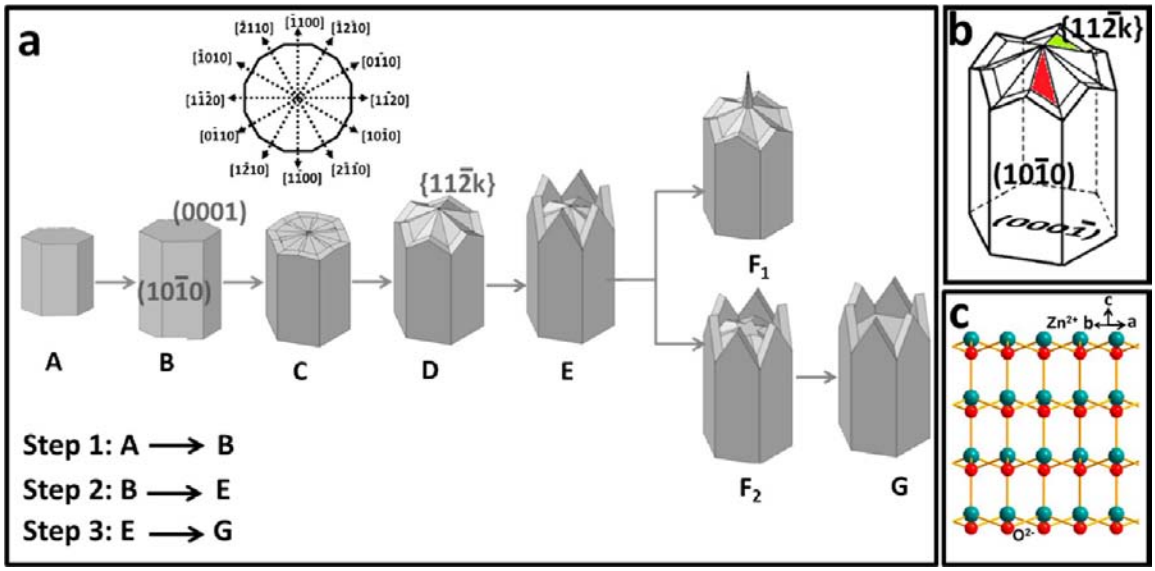

Figure 8. (a) Schematic illustration of the three-step growth mechanism for the formation of the hexagonal crown-capped ZnO micro rods. (b) Schematic model of an intermediate of ZnO with inner fine structure, supposing that the central point and vertex of triangle nanowalls have the same height. (c) Structure model of ZnO projected along [01$\bar{1}$0], showing the termination effect of the crystal.

spectra at the range of 200−500 cm^{-1} using 514 nm laser light (Ar^+ laser) as an excitation source. The Raman signals are usually very sensitive to the crystal structure as well as their inner defects. Based on the group theory analysis, at the Γ point of the Brillouin zone, the $A_1+E_1+2E_2$ modes are Raman active.[17] The main dominant peak labeled as E_2 (high) at about 433 cm^{-1} is known as a Raman-active optical phonon mode, which is the characteristic of wurtzite hexagonal phase ZnO.[18] According to Figure 7, the E_2 (high) peak shows a dominant intensity and a very sharp feature, indicating that the obtained ZnO samples are well-crystallized. It is observed that the E_2 (high) mode becomes stronger with the prolongation of the reaction time, which may be ascribed to improved crystallinity of the prepared ZnO samples. The ZnO sample with the hexagonal crown-capped end obtained after 10 h of incubation exhibits the strongest E_2 (high) peak (Figure 7c). Thus, the hexagonal crown-capped ZnO micro rods have the best crystal quality, which is in agreement with the XRD analysis. From 3 to 10 h, the E_2 (high) mode is blue-shifted a little, which might be due to the optical phonon confinement by nanostructures and anisotropic internal strains corresponding to different growth directions. When the reaction passed 3 h, growth in the [10$\bar{1}$0] and [2$\bar{1}\bar{1}$k] directions turned up, resulting in the blue-shift of the E_2 (high) mode. The peaks at 373 cm^{-1} and 409 cm^{-1}correspond to A_1(TO) and E_1(TO) phonons of ZnO crystal, respectively. The modes E_1(TO), A_1(TO) reflect the strength of the polar lattice bonds.[18a] The peak located at 328 cm^{-1} is the second-order Raman spectrum, originating from the zone-boundary phonons as labeled with E_{2H}-E_{2L} which is a multiphonon scattering process.[18b]

Growth Mechanism. The chemical reactions of the formation of the hexagonal crown-capped ZnO micro rods using the zinc salt/HMT solution have been suggested to be as follows:[19]

$$(CH_2)_6N_4 + 6H_2O \rightarrow 6HCHO + 4NH_3 \quad (1)$$

$$NH_3 + H_2O \rightleftharpoons NH^{4+}OH^- \quad (2)$$

$$2OH^- + Zn^{2+} \rightarrow Zn(OH)_2 \rightarrow ZnO + H_2O \quad (3)$$

ZnO crystals formed both in the solution and on the substrate surface via homogeneous and heterogeneous nucleation, respectively. From the above reaction, Zn^{2+} and OH^- in the solution are the key components that generate ZnO crystals. HMT is a nonionic cyclic tertiary amine, which acts as a bidentate Lewis base that coordinates and bridges two Zn^{2+} ions.[20] When attached to the nonpolar side facets, HMT can facilitate the anisotropic growth in the [0001] direction.[21] HMT also acts as a weak base and PH buffer. It hydrolyzes in water and gradually produces HCHO and NH_3, releasing the strain energy that is associated with its molecular structure, as shown in eqs 1 and 2. Then all of the hydroxide ions reacted with Zn^{2+} while the PH value of the solution remains constant. Finally, $Zn(OH)_2$ dehydrates into ZnO when heated (eq 3).

Here, we divide the whole growth process of the hexagonal crown-capped ZnO micro rods into three steps to explore the growth mechanism. The diagram shown in Figure 8a schematically illustrates the whole growth process. The first step focused on the growth of the hexagonal holders along the [0001] direction bounded with the 6 crystallographic equivalent {10$\bar{1}$0} surfaces, namely, the first 3 h after the start of growth. The morphology was fully consistent with the growth habit of the ZnO ideal crystal model. The relative growth velocities of the ZnO crystals are found to be in the order of [0001] > [01$\bar{1}$0] > [000$\bar{1}$] under hydrothermal conditions.[13b,22] The ZnO crystals were suggested to nucleate via a self-nucleation mechanism, which follow the solution−liquid−solid (SLS) mechanism. The initial grains nucleated at liquid−solid interfaces between the substrate and reaction solutions by heterogeneous nucleation, and then grew to ZnO microcrystals.[23] The first step is a simple process of grain growth. Figure 8a is a schematic diagram showing the whole growth process. As the reaction proceeded, the reactants were consumed gradually, and the concentration decreased accordingly, leading to an untimely solute transportation. Zinc ions and oxygen ions could not completely cover the entire (0001) plane of the ZnO micro rods. Thus, the growth along the

direction [0001] was suppressed. Then the crystals would grow mainly along the 12 directions of $[2\bar{1}\bar{1}0]$ and $[10\bar{1}0]$ which have a lower surface energy.[24] To verify the solute transportation mechanism, a series of growth solution renewal experiments were conducted. And the results confirmed that, the transport rate of growth solution plays a vital role on the formation of hexagonal crown-capped ZnO micro rods (see Supporting Information, Figure S2). These 12 directions are of the same growth velocity (inset in Figure 8a), giving rise to the formation of the dodecagon-shaped disks.[25] At the same time, the growth along the axial direction is still continuing. Furthermore, the as-formed $\{10\bar{1}0\}$ surfaces with large surface areas can absorb more Zn^{2+} and O^{2-} than the interior, resulting in the formation of the 6 convex triangle nanowalls. Because of the space confinement effect of the nanowalls, the radial 12 surfaces cannot spread to form a flat dodecagon-shaped disk, but form a group of symmetry bump planes of $\{11\bar{2}k\}$. This intermediate state of the ZnO crystal with inner fine structure is schematically illustrated in Figure 8b. In this structure, we suppose that the central point and the vertex of the triangle nanwall are in the same horizontal line. Meanwhile, the red triangle and the green one are on the same plane $(11\bar{2}k)$. Therefore, we temporarily depicted these bump planes as $\{11\bar{2}k\}$. Considering the growth velocity [0001] > $[10\bar{1}0]$ > $[2\bar{1}\bar{1}0]$ and solute transportation, these 6 convex triangle nanowalls grow faster than the inner part, forming the structure of **E** shown in Figure 8a. This procedure was identified to be the second step. The third step involved the formation of the flat end of the inner face from **E** to **G**. During the reaction, two intermediates were observed, as shown in Figure 4, corresponding to the schematic diagram $\mathbf{F_1}$ and $\mathbf{F_2}$, respectively. A polar surface is an important characteristic of ZnO. The most common polar surface is the basal plane. The oppositely charged ions produce a positively charged (0001)-Zn and negatively charged $(000\bar{1})$-O polar surface,[26] Figure 8c illustrates the structure model of ZnO projected along $[01\bar{1}0]$, showing the termination effect of the crystal. It was reported that the positively charged (0001)-Zn surfaces are catalytically active while the negatively charged $(000\bar{1})$-O surfaces are chemically inert.[22,27] When the reaction is stopped in a Zn-terminated (0001) surface, which is self-catalytically active and a favorable site for further growth, we will obtain a second growth nanotip along [0001] (see Figure 8a $\mathbf{F_1}$). On the other hand, when the growth stopped in a O-terminated $(000\bar{1})$ surface, according to the Bravais–Friedel law,[28] the final shape of the crystal is determined by the relative growth rate at various crystal planes, which states that high index crystal planes with small interplanar spacing grow faster than low index planes, and thus are not seen in the final shape of the crystal. For ZnO crystals, the (0001) plane is the most likely remaining facet after the growth, and the $\{11\bar{2}k\}$ plane easily disappears from the crystal. With a prolonged growth time, the (0001) plane will grow bigger gradually from the center and overlap the $\{11\bar{2}k\}$ plane forming a hexagonal star pattern (see Figure 8 a $\mathbf{F_2}$). Eventually, the $\{11\bar{2}k\}$ plane will be overlapped totally, and the ZnO crystal shows a hexagonal crown-capped morphology as shown in Figure 8a **G**.

4. PHOTOLUMINESCENCE

The PL spectrum of zinc oxide consists of two emission bands at room temperature. The near-band-edge (NBE) emission is always present as the intrinsic emission, while the deep-level emission (DLE) is usually considered to be related to various intrinsic defects produced during ZnO preparation.[29] Figure 9 shows the PL spectrum of the hexagonal crown-capped ZnO micro rods which was excited by 325 nm UV light from a Xe–Cd lamp at room temperature. As a comparison, the PL spectrum of the hexagonal column-shaped ZnO micro rods is also included. The PL spectra of these two samples exhibited similar features, that is, a dominant UV emission peaked at 382 nm and an extremely weak broad green emission centered at 550 nm. The UV emission is considered as NBE emission resulting from the recombination of free excitons. The full width at half-maximum (fwhm) of the UV emission peaks are as narrow as 12 and 15 nm for the crown-capped and column-shaped ZnO rods, respectively, indicating that these micro rods are of high crystalline quality. It is obvious that the hexagonal crown-capped ZnO have a better crystalline quality and optical quality because of its narrower fwhm, which is consistent with the XRD (Figure 5) and Raman spectra analysis (Figure 7). The green emission belongs to the DLE emission which is attributed to transition in defect states, in particular the singly ionized oxygen vacancies.[30] The quality of ZnO can also be evaluated from the intensity ratio of the two emission peaks.[12e] The intensity ratio of the UV emission to the visible emission of the ZnO samples is 10.25 and 6.62 for the crown-capped and column-shaped ZnO rods, respectively. The intensity ratio of hexagonal crown-capped ZnO is 1.5 times stronger than that of the column-shaped ZnO rods, indicating that the hexagonal crown-capped ZnO microcrystals have a better crystalline quality and a stronger capacity in UV emission which may benefit their applications in UV light-emitting diodes and laser diodes.

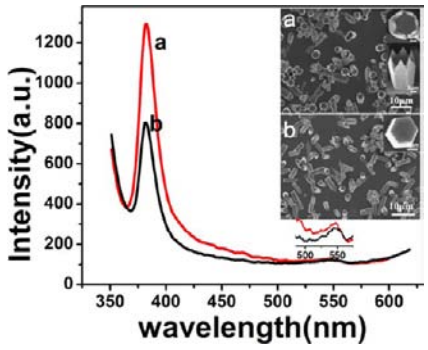

Figure 9. Room-temperature PL spectrum of ZnO samples. (a) The hexagonal crown-capped ZnO micro rods. (b) The hexagonal column-shaped ZnO rods. The excitation wavelength is 325 nm.

The PL spectrum at 90 K was collected to study the low-temperature PL property of the hexagonal crown-capped ZnO micro rods. As can be seen from Figure 10, the low-temperature PL spectrum shows a donor bound exciton (D^0X) emission at 3.345 eV and a weak shoulder on the high-energy side at 3.351 eV which is assigned to the free exciton (FX) emission.[31] The lower-energy side of the D^0X peak has two shoulders located at 3.312 and 3.231 eV, which are attributed to the 1-LO and 2-LO photon replica of FX, respectively. The low-temperature PL spectrum illustrates that the primary emission of the hexagonal crown-capped ZnO micro rods originates from the bound and free exciton recombination.

The temperature-dependent PL spectrum from 100 to 300 K was also collected to better understand the optical property of the hexagonal crown-capped ZnO micro rods (Figure 11). As the temperature increases, the exciton emission shifts to the

dx.doi.org/10.1021/ic401646t | Inorg. Chem. 2013, 52, 10167–10175

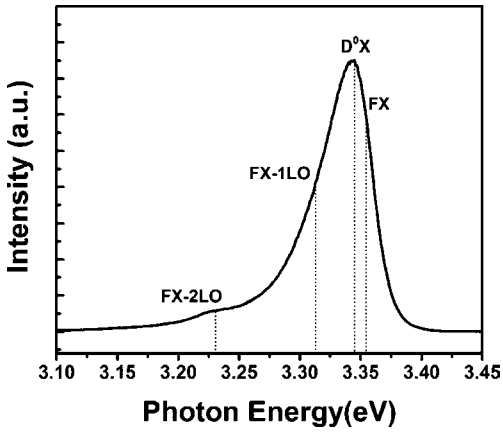

Figure 10. PL spectrum of the hexagonal crown-capped ZnO micro rods at 90 K. The excitation wavelength is 325 nm.

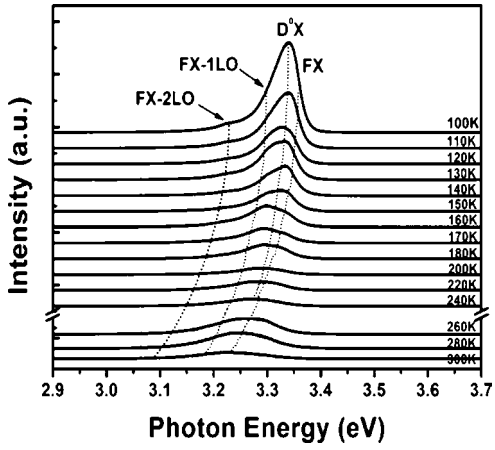

Figure 11. Temperature-dependent PL spectrum of the hexagonal crown-capped ZnO micro rods, the excitation wavelength is 325 nm.

lower energy, and the intensities of all emissions decrease. Compared with the FX emission, the D^0X peak at 3.341 eV loses its intensity more drastically. The decrease in intensity is believed to result from the thermal ionization of the bound excitons.[32] According to Figure 11, the FX emission becomes dominant in the PL spectra when the temperature is over 240 K, indicating that the UV emission at room temperature originates from the free exciton recombination.

5. CONCLUSION

In conclusion, large scale and uniform hexagonal crown-capped ZnO micro rods were fabricated on silicon substrates via a facile low-temperature hydrothermal method without any additives or templates. These ZnO micro rods of new morphology enrich the family of micro- and nanostructured zinc oxides. The XRD, HRTEM, and Raman spectrum of the hexagonal crown-capped ZnO micro rods indicate that they have good crystallinity. The specific growth process and morphology evolution was studied as well as the influence of the reactant concentration on size and shapes. A three-stage growth mechanism from the angle of anisotropic growth and solute transportation was proposed to explain the formation of the crown-capped ZnO micro rods. The room-temperature PL spectrum indicates that the hexagonal crown-capped ZnO microcrystals have a very strong UV emission at 382 nm, while the low-temperature PL spectrum confirms that the primary emission originates from the bound and free exciton recombination. The hexagonal crown-capped ZnO micro rods may find potential applications in field emission devices and enhancing LEE of light emitting diodes.

■ ASSOCIATED CONTENT

Supporting Information

SEM images and analysis on growth solution renewal. This material is available free of charge via the Internet at http://pubs.acs.org.

■ AUTHOR INFORMATION

Corresponding Author

*E-mail: yanqf@mail.tsinghua.edu.cn.

Notes

The authors declare no competing financial interest.

■ ACKNOWLEDGMENTS

The authors are thankful for the financial support from the National Science Foundation of China (No. 51132005 and 51173097) and the National Key Basic Research Program of China (No. 2013CB632902). The Tsinghua National Laboratory for Information Science and Technology (TNList) Cross-discipline Foundation is acknowledged for partial financial support. The authors also thank Professor Q. Li at the Department of Chemistry, Tsinghua University, for fruitful discussions.

■ REFERENCES

(1) (a) Ferry, D. K. *Science* **2008**, *319*, 579−580. (b) Huang, M. H.; Mao, S.; Feick, H.; Yan, H. Q.; Wu, Y. Y.; Kind, H.; Weber, E.; Russo, R.; Yang, P. D. *Science* **2001**, *292*, 1897−1899.

(2) Xia, Y. N.; Yang, P. D.; Sun, Y. G.; Wu, Y. Y.; Mayers, B.; Gates, B.; Yin, Y. D.; Kim, F.; Yan, H. Q. *Adv. Mater.* **2003**, *15*, 353−389.

(3) Ryu, Y.; Lee, T.-S.; Lubguban, J. A.; White, H. W.; Kim, B.-J.; Park, Y.-S.; Youn, C.-J. *Appl. Phys. Lett.* **2006**, *88*, 241108.

(4) Kind, H.; Yan, H. Q.; Messer, B.; Law, M.; Yang, P. D. *Adv. Mater.* **2002**, *14*, 158−160.

(5) (a) Chang, P.-C.; Fan, Z. Y.; Chien, C.-J.; Stichtenoth, D.; Ronning, C.; Lu, J. G. *Appl. Phys. Lett.* **2006**, *89*, 133113. (b) Arnold, M. S.; Avouris, P.; Pan, Z. W.; Wang, Z. L. *J. Phys. Chem. B* **2003**, *107*, 659−663.

(6) Arafat, M. M.; Dinan, B.; Akbar, S. A.; Haseeb, A. S. *Sensors* **2012**, *12*, 7207−7258.

(7) Leschkies, K. S.; Divakar, R.; Basu, J.; Enache-Pommer, E.; Boercker, J. E.; Carter, C. B.; Kortshagen, U. R.; Norris, D. J.; Aydil, E. S. *Nano Lett.* **2007**, *7*, 1793−1798.

(8) Wang, Z. L.; Song, J. H. *Science* **2006**, *312*, 242−246.

(9) (a) An, S. J.; Chae, J. H.; Yi, G. C.; Park, G. H. *Appl. Phys. Lett.* **2008**, *92*, 121108. (b) Jeong, M. C.; Oh, B. Y.; Ham, M. H.; Lee, S. W.; Myoung, J. M. *Small* **2007**, *3*, 568−572.

(10) (a) Zhang, Y. Y.; Ram, M. K.; Stefanakos, E. K.; Goswami, D. Y. *J. Nanomater.* **2012**, *2012*, 1−22. (b) Lee, C. T. *Materials* **2010**, *3*, 2218−2259.

(11) (a) Yu, H. D.; Zhang, Z. P.; Han, M. Y.; Hao, X. T.; Zhu, F. R. *J. Am. Chem. Soc.* **2005**, *127*, 2378−2379. (b) Tak, Y.; Yong, K. J. *J. Phys. Chem. B* **2005**, *109*, 19263−19269.

(12) (a) Wang, Z.; Qian, X. F.; Yin, J.; Zhu, Z. K. *Langmuir* **2004**, *20*, 3441−3448. (b) Wang, Z. L. *Mater. Today* **2004**, *7*, 26−33. (c) Tseng, Y. K.; Huang, C. J.; Cheng, H. M.; Lin, I. N.; Liu, K. S.; Chen, I. C. *Adv. Funct. Mater.* **2003**, *13*, 811−814. (d) Chen, Z.; Shan, Z. W.; Cao, M. S.; Lu, L.; Mao, S. X. *Nanotechnology* **2004**, *15*, 365−369. (e) Yu, Q. J.; Yu, C. L.; Yang, H. B.; Fu, W. Y.; Chang, L. X.; Xu, J.; Wei, R. H.; Li, H. D.; Zhu, H. Y.; Li, M. H.; Zou, G. T. *Inorg. Chem.* **2007**, *46*, 6204−6210. (f) Lao, J. Y.; Huang, J. Y.; Wang, D. Z.; Ren, Z. F. *Nano*

Lett. **2003**, *3*, 235−238. (g) Zhu, G. P.; Xu, C. X.; Zhu, J.; Wang, M. H. *J. Mater. Sci.* **2011**, *46*, 1877−1883.
(13) (a) Liu, D. F.; Xiang, Y. J.; Zhang, Z. X.; Wang, J. X.; Gao, Y.; Song, L.; Liu, L. F.; Dou, X. Y.; Zhao, X. W.; Luo, S. D.; Wang, C. Y.; Zhou, W. Y.; Wang, G.; Xie, S. S. *Nanotechnology* **2005**, *16*, 2665−2669. (b) Li, W. J.; Shi, E. W.; Zhong, W. Z.; Yin, Z. W. *J. Cryst. Growth* **1999**, *203*, 186−196.
(14) Wang, R. C.; Liu, C. P.; Huang, J. L.; Chen, S. J.; Tseng, Y. K.; Kung, S. C. *Appl. Phys. Lett.* **2005**, *87*, 013110.
(15) Laudise, R. A.; Kolb, E. D.; Caporaso, A. J. *J. Am. Ceram. Soc.* **1964**, *47*, 9−12.
(16) (a) Baxter, J. B.; Wu, F.; Aydil, E. S. *Appl. Phys. Lett.* **2003**, *83*, 3797−3799. (b) Wang, R. C.; Liu, C. P.; Huang, J. L. *Appl. Phys. Lett.* **2006**, *89*, 173121.
(17) Arguello, C. A.; Rousseau, D. L.; Porto, S. P. *Phys. Rev.* **1969**, *181*, 1351−1363.
(18) (a) Ashkenov, N.; Mbenkum, B. N.; Bundesmann, C.; Riede, V.; Lorenz, M.; Spemann, D.; Kaidashev, E. M.; Kasic, A.; Schubert, M.; Grundmann, M. *J. Appl. Phys.* **2003**, *93*, 126−133. (b) Khan, A. *J. Pak. Mater. Soc.* **2010**, *4*, 5−9.
(19) (a) Ku, C. H.; Wu, J. J. *J. Phys. Chem. B* **2006**, *110*, 12981−12985. (b) Sun, Y.; Riley, D. J.; Ashfold, M. N. R. *J. Phys. Chem. B* **2006**, *110*, 15186−15192.
(20) Ahuja, I. S.; Yadava, C. L.; Singh, R. *J. Mol. Struct.* **1982**, *81*, 229−234.
(21) Sugunan, A.; Warad, H. C.; Boman, M.; Dutta, J. *J. Sol-Gel Sci. Technol.* **2006**, *39*, 49−56.
(22) Umar, A.; Hahn, Y. B. *Appl. Phys. Lett.* **2006**, *88*, 173120−173121.
(23) (a) Trentler, T. J.; Hickman, K. M.; Goel, S. C.; Viano, A. M.; Gibbons, P. C.; Buhro, W. E. *Science* **1995**, *270*, 1791−1794. (b) Le, H. Q.; Chua, S. J.; Koh, Y. W.; Loh, K. P.; Chen, Z.; Thompson, C. V.; Fitzgerald, E. A. *Appl. Phys. Lett.* **2005**, *87*, 101908.
(24) Wang, Z. L.; Kong, X. Y.; Ding, Y.; Gao, P. X.; Hughes, W. L.; Yang, R.; Zhang, Y. *Adv. Funct. Mater.* **2004**, *14*, 943−956.
(25) (a) Liu, J.; Zhang, Y.; Qi, J. J.; Huang, Y. H.; Zhang, X. M.; Liao, Q. L. *Mater. Lett.* **2006**, *60*, 2623−2626. (b) Dai, J.; Xu, C. X.; Gao, M.; Liu, Z.; Shi, Z. L.; Xu, X. Y.; Guo, J. Y.; Li, Z. H. *CrystEngComm* **2012**, *14*, 2180−2185.
(26) Gao, P. X.; Wang, Z. L. *J. Phys. Chem. B* **2004**, *108*, 7534−7537.
(27) Wang, Z.; Kong, X. Y.; Zuo, J. M. *Phys. Rev. Lett.* **2003**, *91*, 185502−1.
(28) Donnay, J. D. H.; Harker, D. *Am. Mineral.* **1937**, *22*, 446−467.
(29) Lin, B.; Fu, Z. X.; Jia, Y. *Appl. Phys. Lett.* **2001**, *79*, 943−945.
(30) Yu, S. Y.; Zhang, H. J.; Peng, Z. P.; Sun, L. N.; Shi, W. D. *Inorg. Chem.* **2007**, *46*, 8019−8023.
(31) Wang, D.; Liu, Y. C.; Mu, R.; Zhang, J. Y.; Lu, Y. M.; Shen, D. Z.; Fan, X. W. *J. Phys.: Condens. Matter* **2004**, *16*, 4635−4642.
(32) Hamby, D. W.; Lucca, D. A.; Klopfstein, M. J.; Cantwell, G. *J. Appl. Phys.* **2003**, *93*, 3214−3217.